

Single Particle Carbon Combustion

by

Joseph H. Cerv

B.S., United States Military Academy, 1978

---

A MASTER'S THESIS

submitted in partial fulfillment of the  
requirement for the degree

MASTER OF SCIENCE

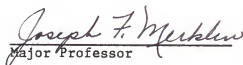
Department of Nuclear Engineering

KANSAS STATE UNIVERSITY

Manhattan, Kansas

1985

Approved by:

  
Major Professor

LD  
2668  
.74  
1985  
C47  
c.2

	<u>Page</u>
LIST OF FIGURES . . . . .	ii
LIST OF TABLES . . . . .	iii
ACKNOWLEDGEMENTS . . . . .	iv
I. INTRODUCTION . . . . .	1
II. EXPERIMENTAL . . . . .	6
II.A Equipment . . . . .	6
II.B Experimental Procedure . . . . .	15
II.C Uncertainty Analysis . . . . .	19
III. RESULTS . . . . .	21
III.A Power Study . . . . .	21
III.B Ambient Effect . . . . .	26
III.C Soaking Effect . . . . .	31
IV. DISCUSSION . . . . .	40
IV.A Theory . . . . .	40
IV.B Comparison with Data . . . . .	45
IV.C Comparison Result . . . . .	46
V. CONCLUSIONS . . . . .	47
APPENDIX A. Particle Heat-up and Steady-State Temperature . . . . .	48
APPENDIX B. Ungraphed Data . . . . .	51
APPENDIX C. Approximation of $\lambda R$ . . . . .	54
APPENDIX D. Mass Loss from Pore Oxygen . . . . .	58
APPENDIX E. Electrode Carbon Test . . . . .	59
REFERENCES . . . . .	64

## LIST OF FIGURES

<u>Figure</u>		<u>Page</u>
1	Exploded View of Quadrupole. . . . .	7
2	Cross Section of Quadrupole. . . . .	8
3	Circuitry for Quadrupole . . . . .	11
4	Combustion Optics. . . . .	13
5	Experimental Set-up. . . . .	14
6	Power Test Swelling Data . . . . .	23
7	Power Test Mass Loss Data. . . . .	25
8	Ambient Effect Swelling Data . . . . .	28
9	Ambient Effect Mass Los Data . . . . .	30
10	Soaking Effect Swelling Data Air Ambient . . . . .	33
11	Soaking Effect Mass Loss Data Air Ambient. . . . .	35
12	Soaking Effect Swelling Data Oxygen Ambient. . . . .	37
13	Soaking Effect Mass Loss Data Oxygen Ambient . . . . .	39
14	Electrode Carbon Swelling Data . . . . .	61
15	Electrode Carbon Mass Loss Data. . . . .	63

LIST OF TABLES

<u>Table</u>		<u>Page</u>
1	Shutter Calibration. . . . .	12

### Acknowledgements

Fred Merklin who put me on the right road.

Chris Sorensen who made me keep asking myself if I was still on it.

My lovely wife, Mary, who bankrolled this endeavor both materially and spiritually.

Engineering Experiment Station, College of Engineering, Kansas State University, Grant Number 0607.

## I. Introduction

Theoretically, the oxidation of carbon has been one of the most intensely considered topics in the field of combustion. Experimentally, the data on carbon combustion, especially for small particles, is lacking. The major studies and experiments with carbon sphere combustion are as follows.

In 1924, Nusselt proposed his "shrinking drop" model for the combustion of a solid sphere such as wood or coal. This model assumes that oxidation occurs only at the surface producing CO and/or CO<sub>2</sub> and that the internal temperature history is governed strictly by a 1-dimensional conduction equation. When a point on the sphere reaches a characteristic pyrolysis temperature it is assumed to have burned. While this model was a start, it failed for several reasons. It ignored temperature dependence of reaction rates, stoichiometry, diffusion limits, and ash effects.<sup>1</sup>

In 1931, Burke and Schumann assumed that pure carbon is consumed due to the reaction with CO<sub>2</sub> at the surface to form CO. The CO thus formed reacts with the surrounding oxygen at a flame sheet to form CO<sub>2</sub>. The CO<sub>2</sub> thus formed at the flame sheet then diffused back to the surface to sustain the process. Burke and Schumann showed the importance of stoichiometric considerations in the problem.<sup>2</sup>

In 1951, Spalding developed the principles of liquid drop combustion which used an evaporative vapor-phase diffusion flame to describe the combustion of droplets. While this model adequately described several solid and liquid combustion systems, it failed in the case of carbon. Due to the high sublimation temperature of carbon which

is 3800°K, it really does not have a significant vapor phase concentration at realistic combustion temperatures.<sup>3</sup>

In 1958, Coffin developed a system for determining the steady state burning rate of solids utilizing mass transfer coefficients rather than vapor phase diffusion. Using this method, he was able to effectively model for the cases in which the mass transfer processes are rate-determining.<sup>4</sup>

The late 1970's brought expensive oil and a greatly renewed interest in coal combustion. This factor, coupled with an explosive increase in the availability of computational facilities, spawned several computer model studies. Principle among the computer model studies was the one by Libby and Blake.

Laurendeau, in his tome Heterogeneous Kinetics of Coal Char Gasification and Combustion, covered all aspects of the topic; coal and char characteristics, surface mechanisms, particle reaction models, and kinetics of char gasification and combustion. Of principle interest in this study is the comparison of the Shrinking Drop Model which assumes a strictly surface reaction to the Progressive Conversion Model which considers pore effects. For small particles on the order of tens of microns, there is considerable question as to which is the proper mechanism.<sup>5</sup>

Libby and Blake, using a computer model of a single coal particle that considered ash effects and reaction rates as well as diffusion, established the concept of an extinction diameter. The extinction diameter is the particle size at which a burning particle's heat loss exceeds its heat production. At the extinction diameter the particle extinguishes itself.<sup>6,7</sup>

Experimentally, the literature is sparse. In the 1930's studies were done by Tu, Hottel and Davis to determine the combustion rate of carbon. Large spheres (2.5 cm in diameter) and carbon samples in cups were heated in furnaces, the mass loss rates were measured and the gas profiles around the carbon bodies were sampled. These experiments validated Burke and Schumann's idea of the flame front for large particles. However, it must be remembered that this work was conducted with large particles.<sup>8,9,10</sup>

Experimental work in the area of individual coal particle combustion slowed in the 1940's as pulverized coal began being used as a fuel in boilers. Interest shifted to furnace design with large groups of interacting particles. Sherman in 1940 analyzed the space requirement for pulverized fuel combustion using an entrained flow of coal particles through a furnace.<sup>11</sup> Even though data was needed on individual small particles, it was not until 1976 that work in this area was conducted.

In 1976, Ubhayakar and Williams studied the burning rate of small carbon particles (50  $\mu\text{m}$  - 200  $\mu\text{m}$ ). The particles were suspended on a quartz fiber with grease and ignited with a pulse from a ruby laser. As the particle ignited, it fell from the quartz fiber and was followed by a high speed camera. Additionally, two color pyrometry gave a temperature history.<sup>12</sup> Results showed that for 50-200  $\mu\text{m}$  particles the flame sheet idea is not valid and the flame is confined to the particle surface. Additionally, particle extinction was experimentally verified.

Since the study by Ubhayakar, high speed cinematography and two-color pyrometry have been used in several studies that follow particles through a furnace. This system gives burnout times and temperature histories for 50-100  $\mu\text{m}$  particles.<sup>13,14</sup>



Real boilers use fuel sieved through 200 (74  $\mu\text{m}$ ) or 400 (37  $\mu\text{m}$ ) meshes. This gives a size distribution weighted in the 20-50  $\mu\text{m}$  range. Studies have not been conducted on this size carbon particle because up to now, there has not been an experimental method by which they could be measured. In the past 15 years a new version of an old device, the modified Milliken Cell, has been developed that can isolate, hold, and weigh these sizes of particles.

The bihyperboidal Milliken cell was first developed in 1970 at Aberdeen Proving Ground to provide a method for isolating and observing 20 to 100  $\mu\text{m}$  aerosol particles.<sup>15</sup> In 1981, Arnold developed the concept of electron-stepping as a method of mass and charge measurement. This concept is based upon the fact that if a charged particle lost an electron, the particle mass and charge can be determined from two voltage measurements. Arnold applied this concept to a flat plate Milliken cell and was able to weigh picogram size particles.<sup>16</sup> In 1982, Philip, et al., showed that the technique of electron stepping could also be used in the bi-hyperboidal Milliken cell and an extremely sensitive mass isolation and measuring device was available.<sup>17</sup> It has the capability of capturing and holding a particle at one position in space and it can weigh particles in a mass range from  $10^{-8}$  g to  $10^{-12}$  g. Since 1981, the bihyperboidal Millikan cell or quadrupole has been a piece of equipment in search of a use.

The objectives of this study were to extend the data on carbon particles into the range of 10 to 50  $\mu\text{m}$  and to study the absolute changes in these particles caused by the combustion process. The Milliken Cell allows a direct measurement of mass and size changes for these particles. Because absolute size and mass change data are

available through this method, evaluation of the two principal small particle combustion models is possible. Data collected in this experiment shows that for 20-50  $\mu\text{m}$  carbon graphite particles a progressive conversion model that includes pore diffusion is preferred over a shrinking core model that ignores pore diffusion.

## II. Experimental

The experimental equipment and technique for mass determination followed as closely as possible that used by Philip, et al.<sup>18</sup>

### A. Equipment

#### 1. Quadrupole (Modified Milliken Cell)

The quadrupole, shown in Figs. 1 and 2, that suspends the particles has surfaces defined by the following equations. The inner surfaces of the endcap electrodes are given by

$$z^2 = \frac{r^2}{2} + Z_0^2, \quad (1)$$

where  $Z_0 = 4$  mm and is the vertical distance from the geometric center of the chamber and  $r$  is the radial distance from the axis of symmetry. The characteristic dimension of the chamber is  $Z_0$ , half the distance between the two end-cap electrodes, measured along the axis of symmetry. The inner surface of the ring electrode is described by

$$z^2 = \frac{r^2}{2} - Z_0^2. \quad (2)$$

The quadrupole with insulating spacers used in this study was fabricated by Temco Corporation, Danvers, Mass.

The chamber consisted of a central ring electrode of aluminum and two teflon rings on either side. The two aluminum endcap electrodes were mounted in the teflon rings. Ten (1/8") access ports were drilled into the teflon rings between the ring and end-cap electrodes. All access ports could be sealed by flat glass windows when not in use. All outside metal surfaces on the quadrupole were covered with teflon shields to prevent electrical shock.

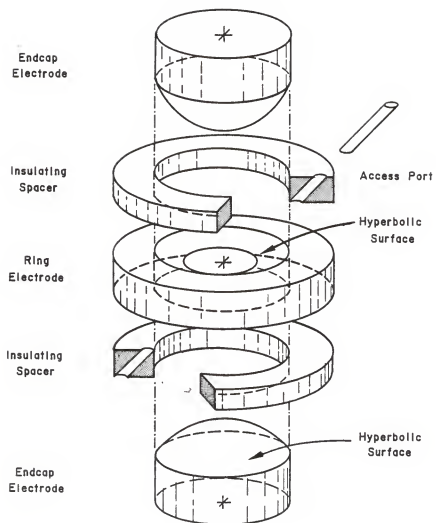


Fig. 1 Exploded view of Quadrupole

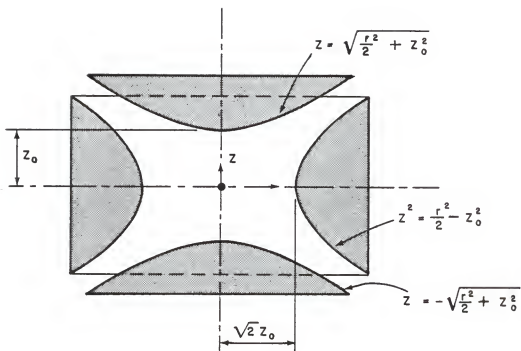


Fig. 2 Cross-section of Quadrupole

## 2. Circuitry

The circuitry to produce the ac voltage (with dc bias) on the ring electrode and the dc voltage across the endcaps is given in Fig. 3. The capacitor-resistor network suppresses induced ac voltages on the endcap electrode resulting from the ac voltage on the ring electrode. The regulated dc power supply to produce  $V_g$  across the end-caps consists of a Pacific Instruments 7104 PC card. This card is capable of producing 0-2000 V across the end-caps with a resolution of 0.0005 V. The power transformers were Essex Stancor P-8151 2400 VAC CRT transformers. The power transformers were controlled by a Powerstat T/16 non-grounded variable transformer. The ring electrode system provided an rms ac voltage of 0 to 4800 V at 60 HZ with a resolution of about 50 V. Measurements of  $V_g$  were made with a Keithly 192 digital multimeter capable of reading up to  $6\frac{1}{2}$  digits. The meter was protected by a 30 A fuse on the negative lead.

## 3. Illumination, Particle Sizing and Electron Stepping

Illumination was provided by a Spectra Physics Model 102-3 helium-neon laser. The laser was mounted on a single axis translational stage and attached to a lead brick. This mounting coupled with a beam steerer allowed the laser beam to be directed into the chamber along the asymptote between the electrodes. The particles were observed and sized through a flat glass window at  $23^\circ$  to the illuminating beam using a Beck telescope with an image distance of 200 mm, a 50 mm objective, and a 10X Beck micrometer eyepiece. Sizing was accomplished by sweeping the movable reticle across the particle image. Adjusting the ac field to align one edge of the particle with the stationary stadia line gave best results. This optical system allowed a resolution of 2.5  $\mu\text{m}$  in sizing particles.

The UV light for electron stepping was provided by an Oriel 6035 low pressure mercury calibration lamp. The lamp was mounted in one of the ten chamber access ports.

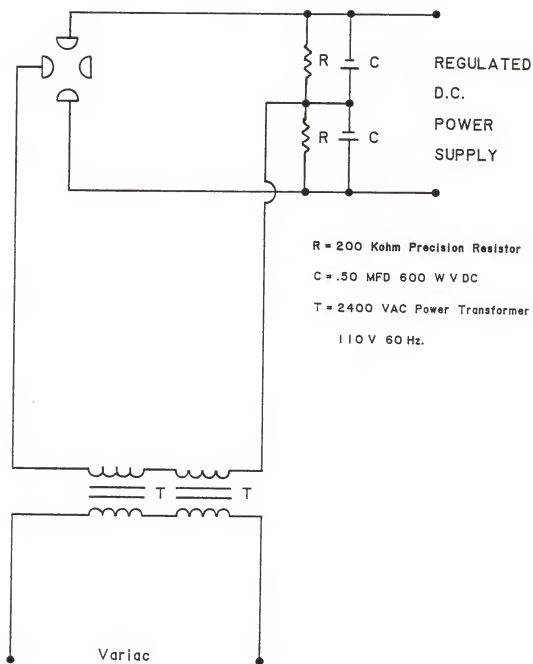


Fig. 3 Circuitry for Quadrupole



#### 4. Combustion Optics (Fig. 4)

Energy is delivered to the particle in the following manner. A 5 W Spectra-Physics Argon Laser provided a beam at wavelength of 514.5 nm. This beam was split and focused upon the particle as two beams 180° apart from each other through 1/8" holes drilled in the ring electrode. The beams were focused by 100 mm lenses to achieve, for a 0.5 watt beam, a power density on the order of  $10^8$  W/m<sup>2</sup> and a heating rate of  $10^6$  °K/sec. See Appendix A. Exposure time was controlled by a camera shutter. The shutter was calibrated using a cadmium photoresistor and a memory oscilloscope. Actual times are shown in Table 1.

Table 1. Shutter Calibration

<u>Shutter Setting</u>	<u>Time (actual)</u>
10	145.4 ms
25	61.7 ms
50	28.1 ms
100	13.4 ms
300	5.76 ms

The overall experimental schematic is shown in Fig. 5.

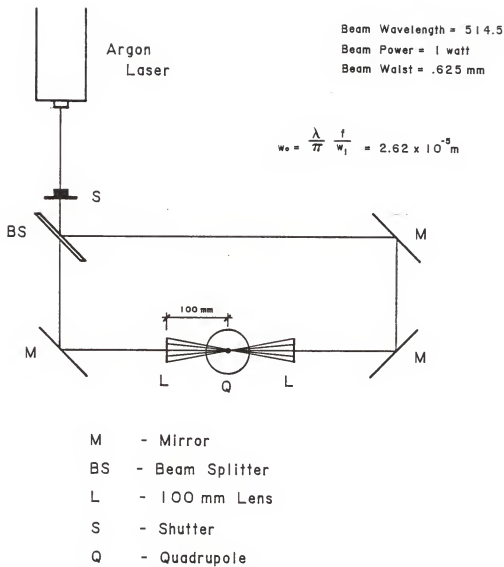


Fig. 4 Combustion Optics



## B. Experimental Procedures

### 1. Mass Measurement

#### a.) Data Collection

The ring voltage was initially adjusted to about 500 V. The voltage across the end-caps was set to its minimum value, typically about .025 V. Particles were injected into the chamber with a hypodermic needle. Due to the applied A.C. field in the ring electrode, this often left several charged particles stably oscillating in the quadrupole. Then a particle that responded suitably to the balancing D.C. voltage was balanced at the center of the chamber. A stationary particle was assumed to be balanced since any departure from the center of the chamber resulted in oscillations of the particle. The ring ac voltage was then lowered for a few seconds. This usually allowed the unbalanced particles to fall out of the chamber while the balanced particle remained near the chamber center. The ac voltage was then increased again. The remaining particle was more carefully balanced by adjusting  $V_g$  and then lowering the ac voltage for a couple of seconds. If the particle drifted from the chamber center, it was clearly unbalanced. The ring voltage was then increased again and  $V_g$  further adjusted, after which the procedure was repeated, until, on lowering and raising the ac voltage the particle remained stable. The UV light was then turned on for an instant. Electron loss was verified by lowering the ac voltage and observing particle drift. The particle was then re-balanced at the chamber center by the technique already described and  $V_g$  recorded again. This procedure is repeated a number of times and from several measurements of  $V_g$  the mass and charge of the particle can be calculated.

b) Mass Calculation<sup>19</sup>

For a stationary particle at the center of the quadrupole, a simple force balance describes the mass of the particle as

$$m = \frac{C q V_g}{g Z_o} \quad (3)$$

where  $q$  is particle charge,  
 $C$  is the geometric constant for the chamber equal to 0.4,  
 $g$  is the gravitational constant,  
 $Z$  is the characteristic dimension of the quadrupole  $Z_o = 4 \text{ mm}$ ,  
 and  $V_g$  is the potential difference across the end-caps.

The charge on the particle equals the number of excess electrons times the charge on an electron so

$$m = \frac{C n e^{-} V_g}{g Z_o} \quad (4)$$

Collecting constants

$$m = K n V, \quad (5)$$

where  $K = \frac{C e}{g Z_o} = 1.6356 \times 10^{-15} \text{ g/V}$ .

If  $V_n$  and  $V_{n+1}$  represent the balancing voltages for a particle containing  $n$  and  $n+1$  excess electrons, respectively, then by solving the previous equation at each balancing voltage the particle mass is given by

$$m = K \frac{V_n V_{n+1}}{V_n - V_{n+1}} \quad (6)$$

For relatively large particles ( $10^{-8} \text{ g}$ ) with large numbers of excess electrons ( $10^5$ ) over a small range of voltage (1V) this can be approximated as

$$m = K \frac{\bar{v}^2}{\Delta V \text{ for a single electron}} \quad (7)$$

The problem is now reduced to finding the voltage change for a single electron.

Given a sample series of voltage measurements a first order difference table is set up.

$$\begin{array}{r} 312.824 \\ 313.188 > .294 \\ 313.346 > .228 \\ 313.463 > .117 \\ 313.559 > .096 \\ 313.601 > .042 \\ 313.830 > .231 \end{array} \quad (8)$$

This was the standard method used by Milliken in his work.<sup>20,21</sup> From here Milliken extracted the voltages that intuitively looked right. This method is unsatisfactory. It is too subjective. An objective quantified method was developed to deal with the problem. Possible values of  $\Delta V$  were tested for fit.

For example, assuming various values of  $\Delta V$  for a single electron loss for the given data and dividing the differences from Eq. (8)

$\Delta V$	<u>.003</u>	<u>.004</u>	<u>.005</u>	<u>.006</u>	<u>.009</u>	
	98.00	73.50	58.80	49.00	32.67	
	76.00	57.00	45.60	38.00	25.33	
	39.00	28.25	23.40	19.50	13.00	(9)
	32.00	24.00	19.20	16.00	10.60	
	14.00	10.50	8.40	7.00	4.67	
	<u>77.00</u>	<u>57.75</u>	<u>46.20</u>	<u>38.50</u>	<u>25.67</u>	
Residual	.00	1.50	1.80	1.00	1.93	

From these tests it is clear that the voltage change for a loss of a single electron is .003 volts, since that value gives the smallest residual.

In this case, from Eq. (7)

$$m = (313.391)^2 / .003 \times 1.635 \times 10^{-15} \quad (10)$$

$$m = 5.3546 \times 10^{-8} \text{ g} . \quad (11)$$

## 2. Sample Preparation

The carbon particles for the test were obtained by filing a piece of CS-312 nuclear-grade graphite and sieving the result through a 400 mesh (37  $\mu\text{m}$ ). The resulting powder ranged from 10 to 50  $\mu\text{m}$ . The density of the particles was measured as follows. A 101 mm x 101 mm x 151 mm block of graphite was weighted at 2643.25 g. The resulting density was 1.748 g/cm<sup>3</sup>. It was assumed that the ground particles have the same density as the block. Since the density of graphite is 2.25 g/cm<sup>3</sup>, the particles were about 22% porous.

Since the particles were porous, an attempt was made to backfill the pores with oxygen. Particles were placed in a vacuum for two days, then under a pressure of two atmospheres in oxygen for another two days. The particles were placed under a vacuum or "outgassed" for two reasons. First, to remove all gas from the macro ( $r > 500 \text{ \AA}$ ) meso ( $20 < r < 500 \text{ \AA}$ ) and micro ( $r < 20 \text{ \AA}$ ) pores; and second, to desorb nitrogen from the active sites on the surface.

After out-gassing, the particles were soaked in oxygen at 2-atmospheres to refill all the pores with oxygen and to establish a monolayer of oxygen on the surface. Once treated, the particles retained a high oxygen concentration for several hours even in an air ambient for the following reasons. Oxygen is chemisorbed and tends to stay on the surface more readily than nitrogen, which is only physically adsorbed. Additionally, it is very difficult for oxygen to escape the

meso and micro pores in the absence of a pressure differential. Since these pores account for approximately 50% of the porosity, oxygen is slow to diffuse from the particles.

Ambient conditions in the quadrupole were changed by flowing 5 cc/sec of gas for 3 minutes. This accomplished approximately 200 changes of gas inside the chamber.

### 3. Measurement Sequence

Measurements were made in the following sequence. Particles were injected into the quadrupole. An ambient atmosphere was established in the quadrupole by flowing gas through it. The gas was turned off. A particle was brought to the center of the chamber by turning off the AC voltage. The particle was stabilized in the center of the chamber and it was sized with the micrometer eyepiece. The mass of the particle was determined by electron stepping as described in Section II-B-1. A laser pulse was impacted upon the particle. The particle was sized. The new particle mass was determined.

### C. Uncertainty Analysis

Consider the sources of uncertainty in the mass calculation,

$$m = K \bar{v}^2 / \Delta V_e ,$$

$$\delta m = \frac{\partial m}{\partial K} \delta K + \frac{\partial m}{\partial \bar{v}} \delta \bar{v} + \frac{\partial m}{\partial \Delta V} \delta \Delta V . \quad (12)$$

K is constant for all mass calculations since it contains only geometric and physical constants. Thus, while K could cause a systematic error it does not introduce any uncertainty from measurement to measurement.



To get the  $\bar{V}$  term,  $V$  is measured over a very small range (1-2V) at a relatively large voltage (300-500V). Therefore, the contribution to the uncertainty of measurement is at most around 1%. For example, in the worst case with a  $\bar{V} = 300$  and a voltage range of 2V,

$$\frac{\partial m}{\partial \bar{V}} \delta \bar{V} = (K/\Delta V_e) 2\bar{V} \delta \bar{V} . \quad (13)$$

The contribution to the uncertainty would be at most 1.2%.

The major source of uncertainty is the determination of  $\Delta V_e$ . Typically, values of  $V_e$  range from .003V to .030V. Since the precision of the voltmeter is  $\pm .001$  V, the effects of a 1 mV voltage uncertainty can be large,

$$\frac{\partial m}{\partial \Delta V} \delta \Delta V_e = (K\bar{V}^2) \frac{1}{\Delta V^2} \delta \Delta V_e . \quad (14)$$

If  $\Delta V_e = 30$  mV, the uncertainty contribution is 3.33%.

If  $\Delta V_e$  is 3 mV, the uncertainty contribution is 33.33%.

The degree to which I can calculate  $\Delta V$  is the key to the accuracy of the measurement. I improve my certainty of  $\Delta V$  in two ways. First, I know the particle size  $\pm 2.5$   $\mu\text{m}$  and I know the density of the material, this gives me a rough estimate of the mass. Second, I rely on several measurements of  $V$  in the determination of  $\Delta V_e$ . The rough knowledge of the mass prevents gross error in the calculation. The use of several voltage measurements cuts the uncertainty of the  $\Delta V_e$  to .0005 V and the uncertainty due to the determination of  $\Delta V_e$  is cut in half.

Depending on the  $\Delta V_e$  magnitude the uncertainty of measurement will range from  $\pm 2\%$  to 18% and that is acceptable.

### III. Results

#### A. Power Study

The first series of runs tested the effect of varying the energy delivered to the particles. Untreated nuclear grade graphite particles were burned in air with decreasing exposure times and beam powers, ranging from shutter speed 015, 1.000 watts to shutter speed 300, 0.007 watts. Three significant items were noted. There was a definite particle swelling, there was a linear relationship between initial mass and the percent mass loss, and there was an ignition cut-off at a low enough laser power. Cut-off power was shutter speed 300, 0.015 watts.

Particle swelling data is shown in Fig. 6. Size increase is generally about 20-30% by volume.

The linear relationship between initial mass and percent mass loss is apparent in Fig. 7. Additionally, note the ignition cut-off, the particles represented by E and F neither swelled or lost mass. Finally, the particles did not burn to completion, they reached an extinction point.

Fig. 6 Power Test Swelling Data

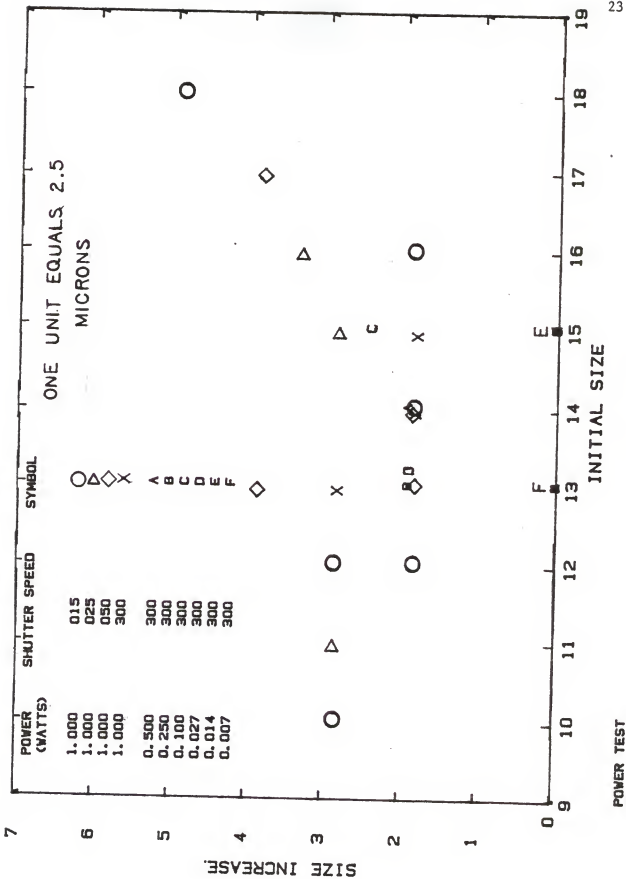


Fig. 7 Power Test Mass Loss Data



## B. Ambient Effect

After the power test was completed, the effects of different ambient atmospheres were explored. Untreated nuclear grade graphite particles were exposed to a 50 shutter setting laser pulse at .50 watts in ambients of pure nitrogen, 50% oxygen/50% nitrogen, and pure oxygen.

The swelling data is presented in Fig. 8. Trends in the data are inconclusive. For particles that ignited, oxygen concentration seems to have little effect upon swelling. Oxygen concentration has a definite effect upon mass loss and this is to be expected from purely diffusional considerations. Figure 9 shows the increase in mass loss, especially for small particles, with increasing oxygen concentration.

Particles in pure nitrogen exhibited neither swelling nor mass loss, one could say they did not ignite.

Fig. 8 Ambient Effect Swelling Data



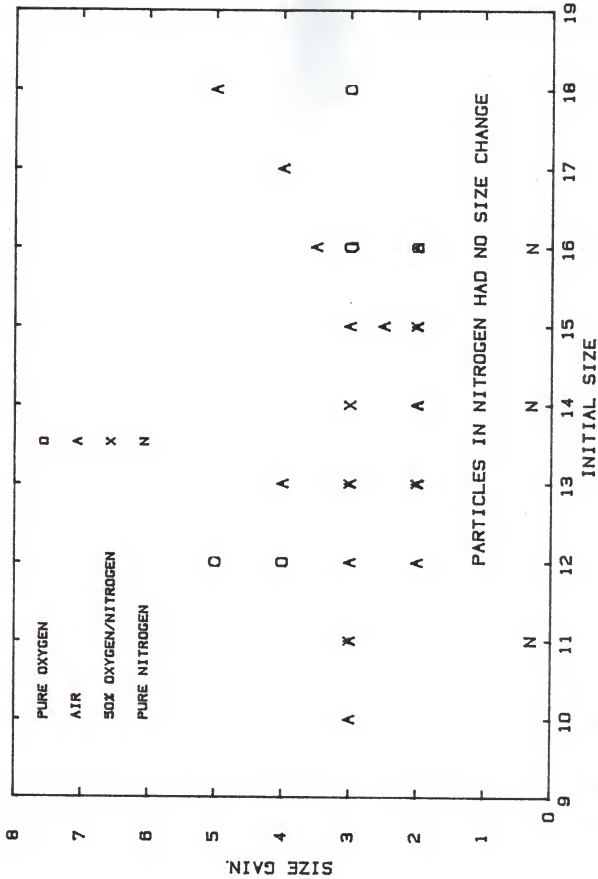
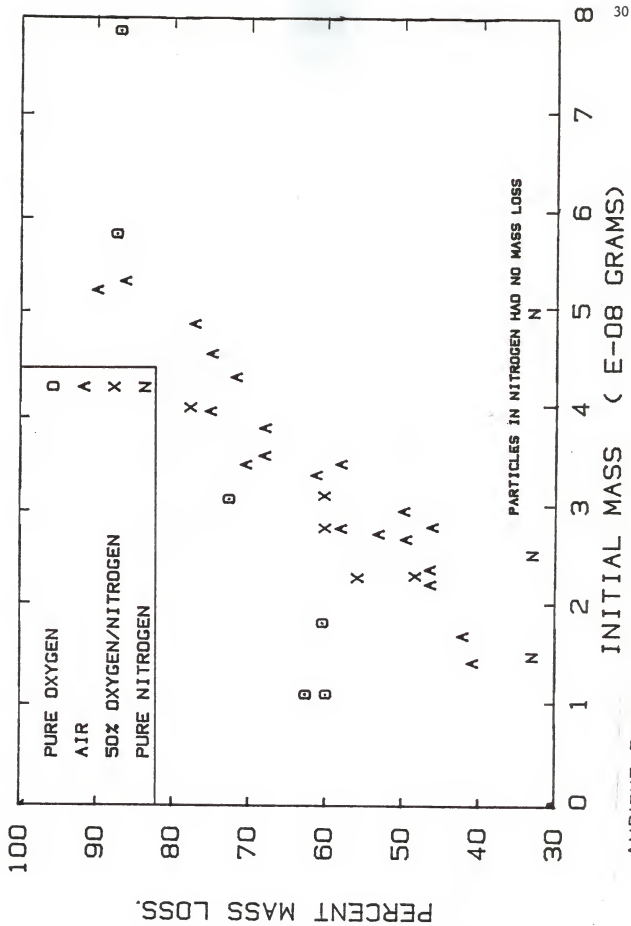


Fig. 9 Ambient Effect Mass Los Data



AMBIENT EFFECT

INITIAL MASS ( E-08 GRAMS)

PARTICLES IN NITROGEN HAD NO MASS LOSS

### C. Soaking Effect

Swelling of pure carbon particles was unexpected. While swelling has been observed in bituminous coal particles during devolatilization, it has not been noted for higher grade coals or graphite.<sup>22</sup> Swelling indicates that there is an interstitial or pore gas effect. This effect was tested by "soaking" particles in oxygen. Nuclear grade graphite particles were treated by exposing them to a vacuum for two days and then back-filling their pores with oxygen by putting the particle under 2 atm of pure oxygen for another two days. Particles were then exposed to a 50 shutter setting laser pulse of .50 watts in ambients of pure nitrogen, air, and pure oxygen.

#### 1. Nitrogen Ambient

In pure nitrogen, oxygen soaking had no effect. Both treated and untreated particles failed to lose mass or to swell.

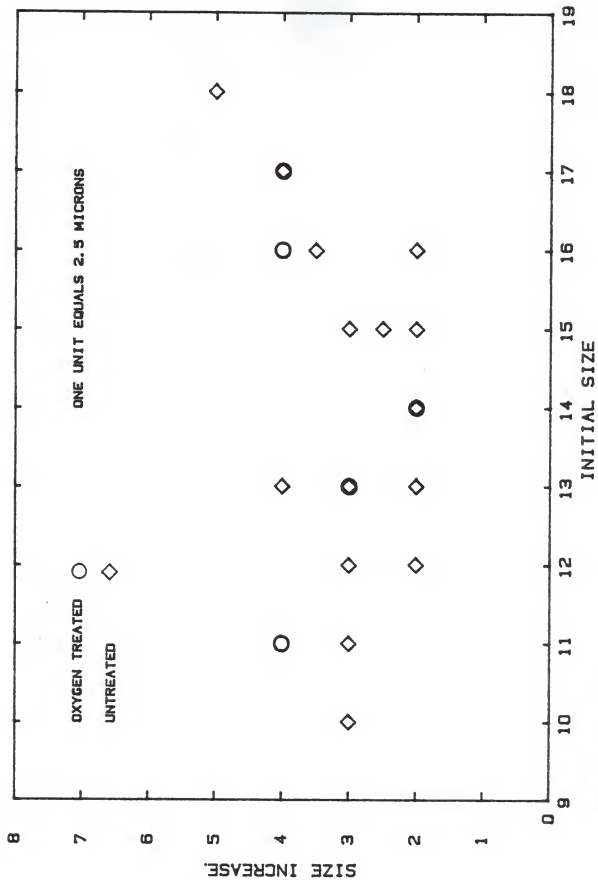
#### 2. Air Ambient

In air, oxygen soaking had a significant effect. As shown in Figures 10 and 11, swelling increases slightly and mass loss significantly increased for the smaller oxygen treated particles.

#### 3. Oxygen Ambient

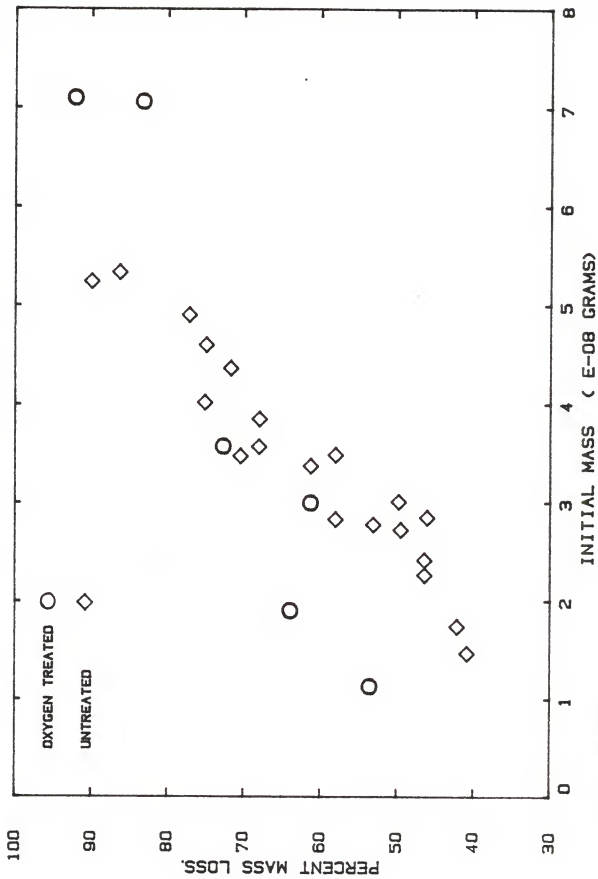
In an oxygen ambient, oxygen soaking has little effect on mass loss, but has a great effect upon swelling. Figures 12 and 13 show the swelling increase and the mass loss comparison for the treated and untreated particles.

Fig. 10 Soaking Effect Swelling Data Air Ambient



SOAKING TEST  
 AIR AMBIENT

Fig. 11 Soaking Effect Mass Loss Data Air Ambient



SOAKING TEST  
AIR AMBIENT



Fig. 12 Soaking Effect Swelling Data Oxygen Ambient

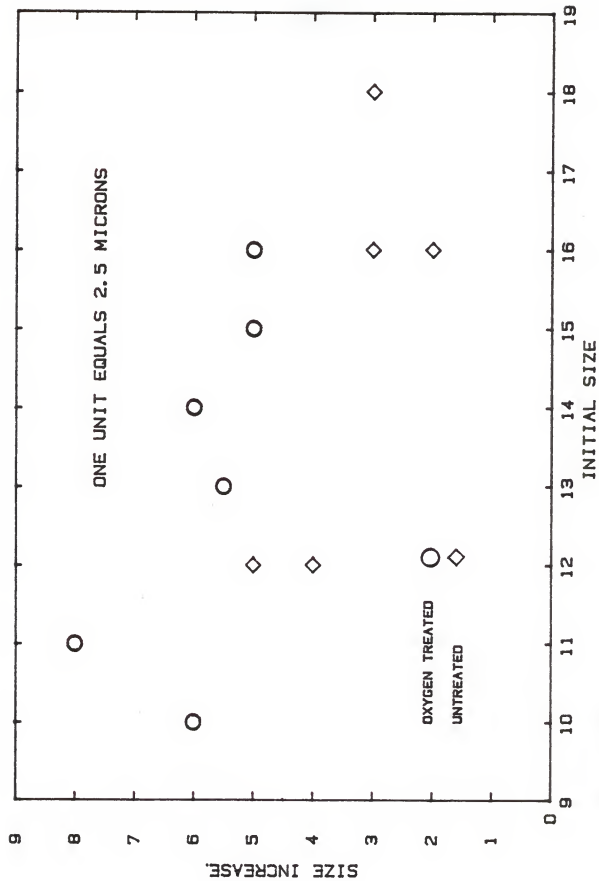
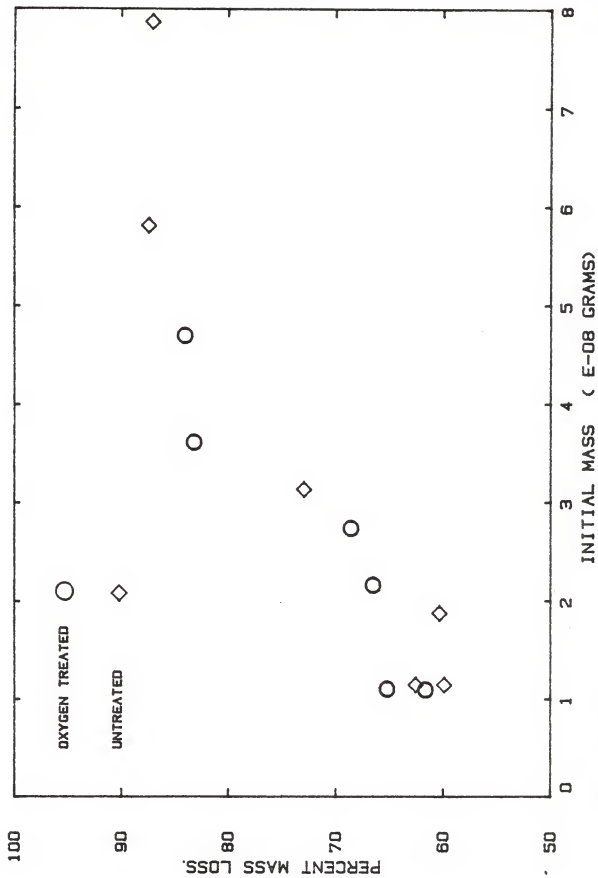


Fig. 13 Soaking Effect Mass Loss Data Oxygen Ambient



SOAKING TEST  
OXYGEN AMBIENT

#### IV. Discussion

The Milliken Cell utilized in this experiment offered a unique way to examine the combustion of carbon. Since absolute values of mass and size were available, direct testing of models is possible. In the following comparison the two principle models for small particle carbon combustion, "the shrinking drop model" and the "progressive conversion model" are compared to the experimental data.

##### A. Theory

###### 1. Diffusional Kinetics

###### a) Shrinking Drop Model

Consider the laser ignition of carbon graphite. The sublimation temperature for graphite is 3800 K so it is not likely that a vapor-phase diffusion flame can exist at realistic combustion temperatures or the temperature achieved in the cell. (App. A). Since there is not a vapor phase diffusion flame the assumption that the chemical kinetic rates are much faster than diffusional rates cannot be made.

Consider a carbon surface burning in a concentration of oxygen in the free stream specified as  $C_{\infty}$ . The burning is at a steady mass rate. If the surface oxidation rate follows first order kinetics and all reactions occur on the surface then

$$G_{ox} = G_f/i = k C_s \quad , \quad (15)$$

where  $G_{ox}$  is the flux of oxygen in gm/sec cm<sup>2</sup>,  $G_f$  is the flux of fuel,  $k$  is the heterogeneous rate constant for surface oxidation reflecting volume to surface area ratio; and  $i$  is the mass stoichiometric index.

The problem is that  $C_s$ , the surface oxygen concentration, is unknown. But, the consumption rate of oxygen must equal the diffusion of oxygen to the surface. Thus, if  $h_o$  is designated the overall convective mass transfer coefficient one can write

$$G_{ox} = k C_s = h_o (C_\infty - C_s) . \quad (16)$$

Seeking the mass burning rate in terms of the free stream oxygen concentration  $C_\infty$ . It follows then that

$$k C_s = h_o C_\infty - h_o C_s , \quad (17)$$

$$k C_s + h_o C_s = h_o C_\infty , \quad (18)$$

$$C_s = \{h_o / (k + h_o)\} C_\infty , \quad (19)$$

or

$$G_{ox} = [\{k h_o / (k + h_o)\} C_\infty] = K C_\infty , \quad (20)$$

where

$$K = k h_o / (k + h_o) , \quad (21)$$

and

$$1/K = (k + h_o) / k h_o = 1/h_o + 1/k . \quad (22)$$

When the kinetic rates are large compared to the diffusion rates  $K = h_o$ ; when diffusion rates are large compared to the kinetic rate  $K = k$ . This describes the shrinking drop case where diffusion into the pores is not considered.<sup>23</sup>

Since pore diffusion is ignored in the shrinking drop model and all reactions are assumed to occur on the surface the following results would be expected in terms of this experiment. For graphite with a low ash content the particle should decrease in size as the graphite is

consumed from the outside in. The mass loss should increase with increasing oxygen concentration. Treating the particle by back-filling its pores with oxygen should have no significant effect upon mass loss or swelling.

#### b) Progressive Conversion

Consider the situation in which diffusion to the particle surface is sufficiently fast that it is not the controlling rate. For the porous medium, carbon is being consumed within the pores as well as on the surface. The surface consumption rates are therefore controlled by kinetic rates; however, the consumption in the pores are controlled by the diffusion of oxygen into the pore.

Thus, the mass consumption rate of oxygen in terms of a flux of oxygen must be that which is consumed at the surface plus that which is consumed in the pores.

$$G_{\text{ox}} = k C_s + D_i \left( \frac{\partial C_i}{\partial n} \right)_s, \quad (23)$$

where  $D_i$  is the internal diffusion coefficient,  $C_i$  is the oxygen concentration inside the particle, and  $n$  is the normal to the surface.

Following the same convention used in the shrinking core development, this equation can be written in the form

$$G_{\text{ox}} = k C_s + D_i \left( \frac{\partial C_i}{\partial n} \right)_s = k' C_s. \quad (24)$$

Using spherical symmetry the internal oxygen diffusion process is described by the equation

$$D_i \left\{ \frac{d^2 C_i}{dr^2} + \frac{2}{r} \frac{dC_i}{dr} \right\} - q = 0, \quad (25)$$

where  $q$  is the oxygen consumption rate per unit particle volume. With the boundary conditions,

$$D_1 \frac{dC}{dr} = h_o (C_\infty - C_s) \text{ at } r = R, \quad (26)$$

$$\frac{dC}{dr} = 0 \text{ at } r = 0. \quad (27)$$

It is possible to express the quantity  $q$  as

$$q = k S_1 C_1 \quad (28)$$

where  $S_1$  is the internal surface area in a particle volume.

The solution of Eq. (25) in terms of the expression as given in Eq. (24) results in the following expression for  $k'$

$$k' = k + \lambda D_1 [\coth(\lambda R) - 1/\lambda R] \quad (29)$$

where  $R$  is the particle radius and

$$\lambda = (S_1 k/D_1)^{1/2} \quad (30)$$

For the case of small values of  $\lambda R$  ( $\lambda R < 0.55$ ) which is physically representative of a small particle  $\coth(\lambda R)$  can be expanded in a series of which only the first two terms are considered significant.<sup>24</sup> See App. C.

$$\coth(\lambda R) = (1/\lambda R + \lambda R/3 - \frac{(\lambda R)^3}{45} + \dots) \quad (31)$$

$$0 < (\lambda R) < \pi$$

Substitution Eq. (31) into Eq. (29)

$$k' = k + \lambda^2 D_1 R/3 = k[1 + S_1 R/3] \quad (32)$$

The expression then is the rate constant when the inner pores participate. Writing this in terms of Eq. (20).



$$G_{OX} = \{[k'h_o/(k' + h_o)]\} C_{\infty} = K C_{\infty} \quad (33)$$

$$K = k'h_o/(k' + h_o). \quad (34)$$

In terms of the progressive conversion model the following experimental results are expected. Since the reactions in pores are considered and the particle burns throughout, the particle should decrease in size only slightly as it burns from the inside out. The mass loss should increase with increasing oxygen concentration. Treating the particle by back-filling its pores with oxygen could have an effect upon mass loss or swelling by initially speeding up the reactions in the pores.

## 2. Extinction

Particle extinction in the sense described by Ubhayakar and Williams and Libby and Blake describes the point at which the heat loss rate of a particle exceeds heat production in the particle and the particle extinguishes itself.<sup>25,26</sup> In the case of the shrinking drop model which is the model used by the above investigators, the extinction condition would exhibit itself in the form of a critical diameter. The critical diameter is the size after which these constant density particle's heat balance went negative.

The progressive conversion model would differ somewhat in its extinction condition. Since the particle burns from the inside out a critical density or a critical mass might be more appropriate, but there would still be a point at which the heat balance went negative and the particle extinguished itself.

## B. Comparison with Data

### 1. Power Test

The power test mass-loss data is consistent with either of these combustion models. Since  $k$  from the Arrhenius Equation, is based upon  $e$ -fold temperature dependence, it is reasonable to see an ignition cut-off in either model. The slope of the data also seems reasonable as the smaller particles are closer to their extinction size and should therefore have less mass loss.

The power test swelling data is not consistent with shrinking drop model. According to the Industrial Engineering Graphite Handbook, the CS 312 graphite utilized in the experiment had an ash content of 0.09%, therefore the low density matrix that remained after the laser heating was essentially pure carbon, not ash.<sup>27</sup> With a surface reaction it is difficult to imagine any mechanism by which swelling could occur.

The power test swelling data can be explained in terms of the progressive conversion model. Internal pressure developed during combustion in the pores combined with the decrease in structural integrity as the particle burns could result in swelling. Additionally, local extinction conditions could be reached in the pores as the particle density decreased giving a porous mass of low density carbon.

### 2. Ambient Test

The ambient test mass-loss data is consistent with both combustion models. Mass loss increases with increasing oxygen concentration and this is consistent with the extinction result predicted by both models.

The ambient test swelling data was inconsistent with the shrinking drop model and could be explained by the progressive conversion model for reasons previously mentioned.

### 3. Soaking Test

The soaking test mass loss data is not consistent with the shrinking drop model. In air, the mass loss increases significantly for treated particles. Since the shrinking drop model ignores the pore effects backfilling those pores should have had very little effect upon mass loss. See Appendix D.

The soaking test results can be explained in terms of the progressive conversion model. Oxygen reacting in the pores would further open the pores at the initiation of the reaction. The additional internal surface area would then increase the reaction rate and the mass loss.

### C. Comparison Result

From the above comparison, the progressive conversion model is preferred. It can be used to explain swelling, and it can explain the increase in mass loss when particles are treated with oxygen. For carbon graphite particles from 20 to 50  $\mu\text{m}$  the progressive conversion model that considers pore diffusion is preferred.

## V. Conclusions

The bihyperboidal Milliken cell has been established as a viable apparatus for studying heterogeneous solid-gas reactions on a single particle basis. Using this device data on carbon particle combustion and extinction was extended into an entirely new size range.

A comparison between the two principle models for small carbon sphere combustion with the data obtained from the Milliken cell shows that one model is clearly favored. For small ( $20\ \mu\text{m} - 50\ \mu\text{m}$ ) carbon graphite particles the progressive conversion model is preferred.

Finally, a standard based upon a known substance, CS312 Nuclear Grade Graphite with known chemical composition and density has been established for future char combustion work with other carbon bearing substances such as coal, wood, etc.

Two further studies are directly suggested by this experiment. First, a computer model study using a constant volume, decreasing density, progressive conversion approach should be done. Second, two-color pyrometry should be coupled with the Milliken Cell to determine particle temperature histories, along with mass and size change data. This additional information would allow a more complete elicitation of the carbon combustion mechanism.

### Appendix A. Particle Heat-up and Steady-State Temperature

In the absence of a chemical reaction the steady state temperature can be approximated using a simple energy balance.

$$q_{\text{Laser}} = q_{\text{conduction}} + q_{\text{radiation}}$$

For a small spherical particle in a large enclosure of air, the following relationships hold at the particle surface.

$$\dot{q}_{\text{cond}} = \frac{4 \pi k_{\text{air}} (T_{\text{sphere}} - T_{\text{ambient}})}{1/R_{\text{sphere}}}$$

$$\dot{q}_{\text{rad}} = \sigma 4 \pi R_{\text{sphere}}^2 \epsilon_{\text{graphite}} (T_{\text{sphere}}^4 - T_{\text{amb}}^4)$$

$$\dot{q}_{\text{Laser}} = \pi R_{\text{sphere}}^2 (\text{Beam Power Density}) (\alpha_{\text{graphite}}) (\text{Mirror Loss})$$

$k_{\text{air}}$  is the thermal conductivity of the air,  $R$  is the particle radius, as shown in Fig. 4, the focused beam waist  $w_0$  is  $2.62 \times 10^{-5}$  m. Thus, for a .5 watt beam the power density is  $2.32 \times 10^8$  w/m<sup>2</sup>. The beam reflects from 4 mirrors and a beam splitter on the way to the particle. Assuming a 10% loss at each surface, the mirror loss term equals  $(.90)^5 = .590$ . Invoking Kirchoff's Law and assuming absorptivity equals emmissivity,  $\alpha = \epsilon = .92$ , power delivered to a 25  $\mu\text{m}$  particle then becomes

$$\begin{aligned} q_{\text{Laser}} &= \pi (12.5 \times 10^{-6})^2 (2.32 \times 10^8) (.92) (.590) \\ &= 6.1816 \times 10^{-2} \text{ watts} \end{aligned}$$

For the same 25  $\mu\text{m}$  particle

$$q_{\text{cond}} = 1.5708 \times 10^{-5} k_{\text{air}} (T_{\text{sphere}} - T_{\text{amb}})$$

$$q_{\text{rad}} = 1.0242 \times 10^{-16} \text{ w/K}^4 (T_{\text{sphere}}^4 - T_{\text{amb}}^4)$$

At T = 2000 K

$$\begin{aligned} q_{\text{cond}} &= (1.5708 \times 10^{-5})(137 \times 10^{-3})(2000 - 300) \\ &= 3.66 \times 10^{-3} \text{ watts} \\ q_{\text{rad}} &= 1.0242 \times 10^{-16} (2000^4 - 300^4) \\ &= 1.6379 \times 10^{-3} \text{ watts} \end{aligned}$$

At T = 2500 K

$$\begin{aligned} q_{\text{cond}} &= (1.5708 \times 10^{-5})(222 \times 10^{-3})(2500 - 300) \\ &= 7.6718 \times 10^{-3} \text{ watts} \\ q_{\text{rad}} &= 1.0242 \times 10^{-16} (2500^4 - 300^4) \\ &= 4.0 \times 10^{-3} \text{ watts} \end{aligned}$$

At T = 3000 K

$$\begin{aligned} q_{\text{cond}} &= (1.5708 \times 10^{-5})(466 \times 10^{-3})(3000 - 300) \\ &= 1.9764 \times 10^{-2} \text{ watts} \\ q_{\text{rad}} &= (1.0242 \times 10^{-16})(3000^4 - 300^4) \\ &= 8.29 \times 10^{-3} \text{ watts} \end{aligned}$$

At T = 3500 K

$$\begin{aligned} q_{\text{cond}} &= (1.5708 \times 10^{-5})(1000 \times 10^{-3})(3500 - 300) \\ &= 5.0266 \times 10^{-2} \text{ watts} \\ q_{\text{rad}} &= (1.0242 \times 10^{-16})(3500^4 - 300^4) \\ &= 1.5369 \times 10^{-2} \text{ watts} \end{aligned}$$

From this very rough calculation it seems that the temperature will stabilize at a maximum temperature of 3400°K. However, there are other loss terms that, while difficult to quantify, are definitely present. The surface of the carbon particles are not smooth, thus both the radiation and conduction loss terms will increase due to increased

surface area. There is a kinetic energy loss. This loss manifests itself in the oscillation of the particle about the field null point when it is irradiated. Oscillations are typically 500  $\mu\text{m}$  from the null point at 60 HZ. Finally, there is the question of aim, these calculations hold only for the center of a Gaussian Beam. Considering the additional loss terms a temperature estimate of 2000°K to 2500°K is probably more accurate.

The initial heating rate can be calculated from the energy equation

$$\begin{aligned} \frac{dT}{dt} &= \frac{q_{\text{Laser}}}{C_{\rho} m_{\text{particle}}} \\ &= \frac{6.1816 \times 10^{-2}}{(709) \frac{1}{6} \pi (25.0 \times 10^{-4})^3 (1.75 \times 10^{-3} \text{ Kg})} \\ &= 6.0897 \times 10^6 \text{ } ^\circ\text{K/sec.} \end{aligned}$$

At this rate heat-up would be very fast reaching 2000°K in 0.33 msec.

## Appendix B. Ungraphed Data

## Power Test Air Ambient

Shutter Speed	Power	S <sub>o</sub>	S <sub>f</sub>	$\times 10^{-8}$ M <sub>o</sub>	$\times 10^8$ M <sub>f</sub>	$\times 10^{-8}$ Δ <sub>m</sub>	Δ <sub>m</sub> %
15	1.000	18	23	3.37	1.31	2.06	61.12
15	1.000	12	15	2.42	1.29	1.13	46.69
15	1.000	16	18	4.60	1.15	3.45	75.00
15	1.000	10	13	2.26	1.21	1.05	46.46
15	1.000	14	16	3.85	1.23	2.62	68.05
15	1.000	12	14	3.48	1.43	2.05	58.91
25	1.000	13	15	1.47	.87	0.60	40.82
25	1.000	17	21	4.90	1.12	3.78	77.14
25	1.000	14	16	4.02	1.00	3.02	75.12
25	1.000	13	17	3.57	1.14	2.43	68.06
50	1.000	15	18	2.72	1.37	1.35	49.63
50	1.000	16	19.5	4.36	1.23	3.13	71.78
50	1.000	11	14	1.74	1.00	0.74	42.52
300	1.000	15	17	2.78	1.30	1.48	53.23
300	1.000	14	16	5.33	.73	4.60	86.30
300	1.000	13	16	2.83	1.19	1.64	57.95
300	.500	14	16	5.24	.526	4.72	89.95
300	.250	13	15	3.47	1.03	2.45	70.41
300	.100	15	17.5	3.01	1.51	1.50	49.78
300	.027	13	15	2.85	1.54	1.31	46.06
300	.014	15	15	5.80	5.80		0
300	.007	13	13	2.82	2.82		0

1 Size unit equals 2.5 μm



Ambient Test

Shutter Speed	Power	S <sub>O</sub>	S <sub>F</sub>	X10 <sup>8</sup> M <sub>O</sub>	X10 <sup>8</sup> M <sub>F</sub>	X10 <sup>8</sup> Δm	Δm%
PURE OXYGEN							
50	.5	12	17	1.14	0.46	0.68	59.84
50	.5	16	18	3.13	0.85	2.28	72.95
50	.5	12	16	1.14	0.43	0.71	62.54
50	.5	19	23	5.81	0.73	5.08	87.42
50	.5	16	19	1.87	0.54	1.13	60.34
50	.5	18	21	7.87	1.01	6.85	87.10
50% OXYGEN/NITROGEN							
50	.7	11	14	2.84	1.13	1.71	60.10
50	.7	13	16	2.33	1.03	1.30	55.82
50	.7	13	15	3.16	1.26	1.90	60.18
50	.7	22	25	12.41	1.38	11.03	88.87
50	.7	14	17	4.06	0.90	3.16	77.71
50	.7	15	17	2.35	1.21	1.14	48.31
PURE NITROGEN							
50	.5	14	14	2.56	2.56	--	0
50	.5	16	16	5.03	5.03	--	0

1 size unit equal 2.5 μm

## Soaking Test

Shutter Speed	Power	S <sub>o</sub>	S <sub>f</sub>	$\times 10^{-8}$ M <sub>o</sub> g	$\times 10^{-8}$ M <sub>f</sub> g	$\times 10^{-8}$ $\Delta m$ g	$\Delta m\%$
PURE OXYGEN							
50	.5	11	19	1.10	0.38	.72	65.4
50	.5	16	21	3.62	0.61	3.09	85.3
50	.5	14	20	2.16	0.72	1.44	66.7
50	.5	10	16	1.09	0.42	0.67	51.5
50	.5	13	18.5	2.74	0.86	1.88	68.6
50	.5	15	20	4.70	0.75	3.95	84.0
AIR							
50	.5	11	15	1.13	0.54	0.59	53.55
50	.5	17	21	7.10	0.56	6.54	92.17
50	.5	16	20	7.06	1.24	5.82	82.37
50	.5	13	16	1.90	0.69	1.21	63.91
50	.5	14	16	3.00	1.15	1.85	61.72
50	.5	13	16	3.57	0.97	2.60	72.67
PURE NITROGEN							
50	.5	14	14	2.56	2.56	--	0
50	.5	13	13	1.62	1.62	--	0
50	.5	16	16	5.25	5.25	--	0

1 size unit equals 2.5  $\mu m$

Appendix C. Approximation of  $\lambda R$ 

$$\lambda = [(S_i k)/D_i]^{1/2}$$

$S_i$  is the internal surface area in a unit particle volume.

$k$  is the heterogeneous reaction rate constant for surface oxidation.

$D_i$  is the internal diffusion coefficient.

$R$  is the particle radius.

R

Assume a 25  $\mu\text{m}$  particle

$$R = 12.5 \times 10^{-4} \text{ cm.}$$

 $S_i$ 

The particle has .22  $\text{cm}^3$  of void per  $\text{cm}^3$  of volume. From the Industrial Graphite Engineering Handbook, an effective pore radius of  $3.2 \times 10^{-4}$  cm can be assumed, therefore assuming cylinders winding through the particle<sup>28</sup> where  $L$  is the total length of the cylinder,

$$L = V_{\text{pores}} / \pi \bar{r}^2,$$

$$L = 6.838 \times 10^5 \text{ cm,}$$

$$\text{and } S_i = L 2\pi\bar{r} = 1.375 \times 10^3 \text{ cm}^2/\text{cm}^3.$$

 $D_i$ 

From the Chemical Engineering Handbook, pore diffusion for a gas can be approximated as<sup>29</sup>

$$D_{\text{pore}} = \frac{\chi}{\tau} \left( \frac{3}{4\bar{r}} \left( \frac{\pi M}{2R\theta} \right) + \frac{1}{D_f} \right)^{-1}$$

where

$\chi$  is the internal porosity of the particles,

$\bar{r}$  is the average pore radius,

$\tau$  is the tortuosity,

$\theta_A$  is the absolute temperature,

$R$  is the gas constant

$M$  is the molecular weight,

and  $D_f$  is the free diffusion constant.

$$\chi = .22$$

$$\bar{r} = 3.2 \times 10^{-4} \text{ cm from Table 5A.08.02 in the Industrial Graphite Engineers Handbook}^{30}$$

$$\tau = 3 \quad \text{Table 5A.08.02}$$

$$M = 32 \text{ g/mole}$$

$$R = (8.314 \times 10^7 \text{ erg/mol } ^\circ\text{K})(1.02 \times 10^{-3} \text{ g cm}^2/\text{erg}) \\ = 8.48 \times 10^4 \text{ g cm}^2/\text{mol } ^\circ\text{K}$$

$$\theta_A = 300 \text{ K to } 3000 \text{ K}$$

$$D_f = .14 \text{ cm}^2/\text{s}$$

$$D_{\text{pore}} = \frac{.22}{3} \left[ \frac{3}{4(3.2 \times 10^{-4})} \left\{ \frac{\pi 32}{2(8.48 \times 10^4)(300)} \right\}^2 + \frac{1}{.14 \text{ cm}^2 \text{ sec}} \right]^{-1}$$

$$D_{\text{pore}} = D_i = 7.026 \times 10^{-3} \text{ cm}^2/\text{sec at } 300^\circ\text{K.}$$

Making the approximation that diffusivity varies with the square root of temperature,

$$D_i(T_1) = \frac{\sqrt{T_1}}{\sqrt{T_0}} D_i(T_0).$$

$$D_i(1500 \text{ K}) = 1.5711 \times 10^{-2} \text{ cm}^2/\text{sec.}$$

$$D_i(3000 \text{ K}) = 2.2218 \times 10^{-2} \text{ cm}^2/\text{sec.}$$

k

Using the kinetic parameters quoted by Libby, the intrinsic reaction rate can be calculated from the following expression

$$R_e = (p_{O_2}) 8710 \text{ g/cm}^2\text{-sec-atm exp}^{-[18 \times 10^3/T]}$$

Assuming 1 atm of oxygen for simplicity,

At 300°K

$$R_e = 7.6269 \times 10^{-23} \text{ g/cm}^2\text{-sec.}$$

At 1500°K

$$R_e = 5.3516 \times 10^{-2} \text{ g/cm}^2\text{-sec.}$$

At 3000°K

$$R_e = 2.159 \times 10^1 \text{ g/cm}^2\text{-sec.}$$

Now

$$R_e = k C_s \text{ and } k = R_e / C_s$$

At 1 atm/300K the density of oxygen is

$$\rho_{O_2} = \left( \frac{MP}{RT} \right) = \left( \frac{82.06 (300)}{(1)(32)} \right)^{-1},$$

$$\rho_{O_2} = 1.299 \times 10^{-3} \text{ g/cm}^3,$$

$$\text{and } k = 5.8714 \times 10^{-20} \text{ cm/sec.}$$

At 1 atm/1500°K,

$$\rho_{O_2} = 2.699 \times 10^{-4} \text{ g/cm}^3,$$

$$\text{and } k = 1.9822 \times 10^2 \text{ cm/sec.}$$

At 1 atm/3000°K,

$$\rho_{O_2} = 1.299 \times 10^{-4} \text{ g/cm}^3,$$

$$\text{and } k = 1.662 \times 10^5 \text{ cm/sec.}$$

Putting terms together

$$\lambda_{300^\circ\text{K}} = \left( \frac{(1.375 \times 10^3)(5.8714 \times 10^{-20})}{(7.026 \times 10^{-3})} \right)^{\frac{1}{2}},$$

$$= 1.0637 \times 10^{-7} \text{ cm}^{-1}$$

$$\lambda_R = 1.3296 \times 10^{-10},$$

$$\lambda_{1500^\circ\text{K}} = \left( \frac{(1.375 \times 10^{-3})(2.699 \times 10^{-4})}{1.5711 \times 10^{-2}} \right)^{\frac{1}{2}}$$

$$= 4.8602 \text{ cm}^{-1}$$

$$\lambda_R = 6.075 \times 10^{-3},$$

$$\lambda_{3000^\circ\text{K}} = \left( \frac{(1.375 \times 10^3)(1.662 \times 10^5)}{2.2218 \times 10^{-2}} \right)^{\frac{1}{2}}$$

$$= 1.0142 \times 10^5 \text{ cm}^{-1}$$

$$\lambda_R = 126.$$

From these rough calculations pore diffusion should be significant through at least 2000°K and the expansion approximation should hold.

## Appendix D. Mass Loss from Pore Oxygen

$$\text{Particle diameter} = 25 \times 10^{-4} \text{ cm.}$$

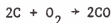
$$\text{Volume} = \frac{1}{6} \pi D^3 = 8.1812 \times 10^{-9} \text{ cm}^3.$$

$$\text{Porosity} = 0.22.$$

$$\begin{aligned} \text{Volume } O_2 &= \text{Porosity} \times \text{Volume} \\ &= 1.7999 \times 10^{-9} \text{ cm}^3. \end{aligned}$$

$$n = \frac{PV}{RT} = \frac{(1 \text{ atm})(1.7999 \times 10^{-9} \text{ cm}^3)}{(82.06 \text{ cm}^3\text{-atm/mole K})(300 \text{ K})}$$

$$n = 7.3113 \times 10^{-14} \text{ mole.}$$



If all internal oxygen reacts

$$1.4623 \times 10^{-13} \text{ moles of carbon will react}$$

$$M_{\text{carbon}} = 12.011 \text{ g/mole}$$

Mass of carbon reacting equals

$$1.7563 \times 10^{-12} \text{ grams.}$$

Typical total mass loss equals  $2.5 \times 10^{-8}$  grams, so mass loss for pore oxygen would be undetectable if it did not affect the combustion process in some way other than being simply consumed.

## Appendix E. Arc Carbon Test

Electrode carbon was burned in air to provide a comparison with Nuclear Grade Graphite.

### Density Determination of Electrode Carbon

Using a Mettler Balance

$$m = 0.2268 \text{ g}$$

Using a Micrometer

$$\text{Diameter} = 0.0984 \text{ in} = .2499 \text{ cm}$$

Using a Meter Stick

$$\text{Length} = 3.50 \text{ cm}$$

$$\text{Volume} = 0.1717 \text{ cm}^3$$

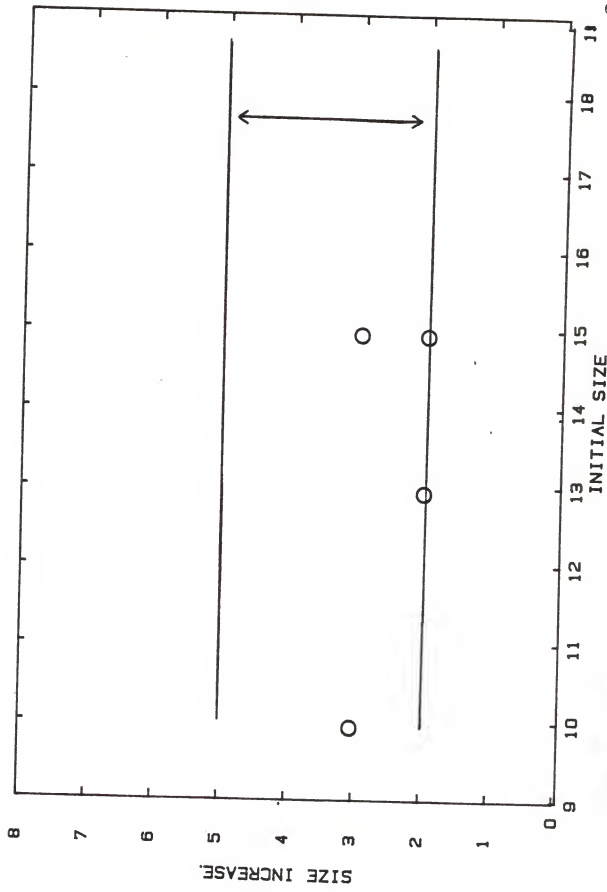
$$\rho = \text{Mass/Volume} = 1.33 \text{ g/cm}^3$$

After grinding and sieving the electrode carbon in the same manner as the Nuclear Grade Graphite, the electrode carbon was burned in the Milliken Cell.

Ranges for Nuclear Grade Graphite particles are shown by lines. Swelling data for the electrode carbon showed the same trends as the swelling data for the Nuclear Grade Graphite with an increase of 20-30% by volume (Fig. 14). Mass loss for the electrode carbon tended to be less than the mass loss for the Nuclear Grade Graphite (Fig. 15). Electrode carbon mass loss ranged from 25% to 72% versus 40% to 90% for the nuclear grade graphite particles with initial masses in the same range. This can be explained by the progressive conversion model in terms of the difference in density between the electrode carbon and the nuclear grade graphite. Because the electrode carbon is less dense, local extinction conditions will be reached sooner, and it will not lose as much mass.

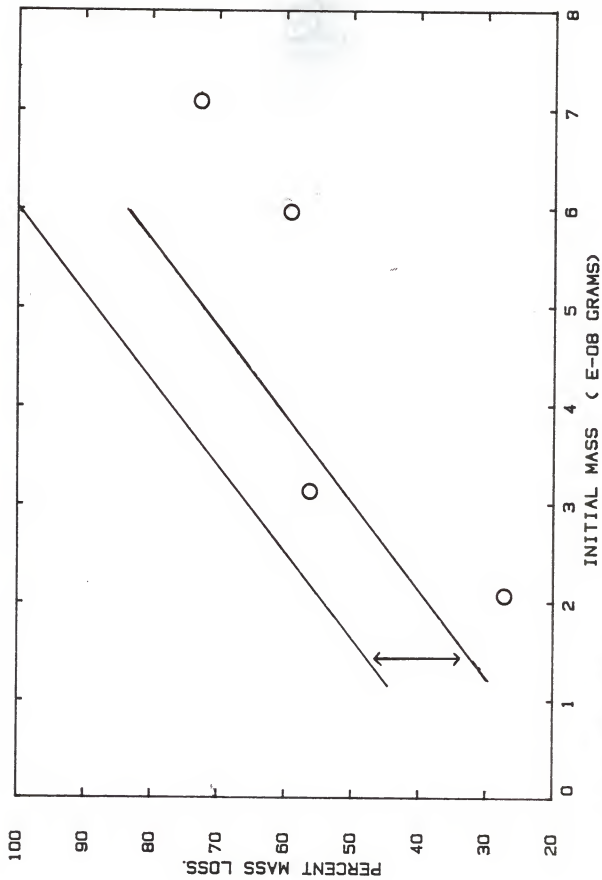


Fig. 14 Electrode Carbon Swelling Data



ELECTRODE CARBON  
AIR AMBIENT

Fig. 15 Electrode Carbon Mass Loss Data



ELECTRODE CARBON  
AIR AMBIENT

## REFERENCES

- <sup>1</sup>Nusselt, W.Z., Ver. Deut. Ing., 68, 124 (1924).
- <sup>2</sup>Burke, S.P. and Schumann, T.E.W., Proceedings 3rd International Conference on Bituminous Coal, 2, 485 (1931).
- <sup>3</sup>Spalding, D.B., Fuel, 30, 121 (1951).
- <sup>4</sup>Coffin, K.P. and Brokaw, R.S., National Advisory Council for Aeronautics, Tech Note 3929 (1957).
- <sup>5</sup>Laurendeau, Normand M., Progressive Energy Combustion Science, 4, 221 (1978).
- <sup>6</sup>Libby, Paul A., Combustion and Flame, 38, 285 (1980).
- <sup>7</sup>Libby, Paul A. and Blake, Thomas, R., Combustion and Flame, 36, 139 (1979).
- <sup>8</sup>Hottel, H.C. and Davis, H., "Combustion Rate of Carbon, Ind. Eng. Chem., 26, 889 (1934).
- <sup>9</sup>Hottel, H.C. and Parker, A.S., Ind. Eng. Chem., 28, 1334 (1936).
- <sup>10</sup>Tu, C.M., Davis, H. and Hottel, H.C., Ind. Eng. Chem., 26, 749 (1934).
- <sup>11</sup>Sherman, R.A., Proc. 3rd International Conf. on Bituminous Coal, 2, 370 (1932).
- <sup>12</sup>Ubhayakar, Shivadev R. and Williams, Forman A., Electrochem. Soc., 123, No. 5, 747 (1976).
- <sup>13</sup>McLean, W.J., Hardesty, D.R. and Pohl, J.H., Eighteenth Symposium (International) on Combustion, Pittsburgh: The Combustion Institute, 1239 (1981).
- <sup>14</sup>Seeker, W.R., et al., "The Thermal Decomposition of Pulverized Coal Particles," Eighteenth Symposium (International) on Combustion, Pittsburgh: The Combustion Institute, 1213 (1981).
- <sup>15</sup>Frickel, Robert H., Shaffer, Roy E. and Stamatoff, James B., "Chambers for the Electrodynamic Containment of Charged Aerosol Particles," Report #ARCSI-TR-77041, Chemical Systems Laboratory, Aberdeen Proving Ground, Maryland 21010 (1970).
- <sup>16</sup>Arnold, Stephen, Journal of Aerosol Science, 10, 49 (1979).
- <sup>17</sup>Philip, Mark A., Gelbard, Fred and Arnold, Stephen, Journal of Colloid and Interface Science, 41, No. 2, 507 (1983).
- <sup>18</sup>Philip, Mark A., Ibid.

- 19 Philip, Mark A., *ibid.*
- 20 Milliken, Robert A., Electrons (+ and -), Chicago: University of Chicago (1918).
- 21 Milliken, Robert A., The Electron, Chicago: University of Chicago (1935).
- 22 McLean, W.J., *ibid.*
- 23 Glassman, Irvin, Combustion, New York: Academic Press (1977).
- 24 Glassman, Irvin, *ibid.*
- 25 Ubhayaker, Shivadev R., *ibid.*
- 26 Libby, *ibid.*
- 27 Industrial Engineering Graphite Handbook, National Carbide Division, Division of Union Carbide (1962).
- 28 Indust. Eng. Graph. Hand., *ibid.*
- 29 Perry, Robert H. and Chilton, Perry C., Chemical Engineering Handbook, 5th Edition, New York: McGraw Hill Book Company, 16-19 (1973).
- 30 Indust. Eng. Graph. Hand., *ibid.*

Single Particle Carbon Combustion

by

Joseph H. Cerv

B.S., United States Military Academy, 1978

---

AN ABSTRACT OF A MASTER'S THESIS

submitted in partial fulfillment of the  
requirement for the degree

MASTER OF SCIENCE

Department of Nuclear Engineering

KANSAS STATE UNIVERSITY

Manhattan, Kansas

1985

## Abstract

Experimental data on the mass loss and size change of a laser-ignited particle of nuclear grade graphite (20 $\mu$ m - 50 $\mu$ m) in quiescent mixtures of oxygen and nitrogen at room temperature are presented. The test variable was the oxygen molar fraction of the ambient environment. A quadrupole allowed absolute measurement of mass for the individual particles, and a linear relationship was found relating initial mass with percent mass loss during the reaction. Additionally, size measurement showed a swelling of 20-30% during the reaction. Two theoretical models, one an unreacted shrinking core model assuming a receding reaction front and the other a progressive conversion model that accounts for particle porosity are considered. Swelling data indicates that the progressive conversion model is the preferred one for (20 - 50  $\mu$ m) graphite particles.